Anomalous dimensions of the Smoluchowski coagulation equation

Jens Eggers
School of Mathematics, University of Bristol, Fry Building, Woodland Road, Bristol BS8 1UG, United Kingdom

Marco Fontelos
Instituto de Ciencias Matemáticas (ICMAT, CSIC-UAM-UCM-UC3M), Campus de Cantoblanco, 28049 Madrid, Spain

(Received 24 August 2023; accepted 9 November 2023; published 5 December 2023)

The coagulation (or aggregation) equation was introduced by Smoluchowski in 1916 to describe the clumping together of colloidal particles through diffusion, but has been used in many different contexts as diverse as physical chemistry, chemical engineering, atmospheric physics, planetary science, and economics. The effectiveness of clumping is described by a kernel $K(x, y)$, which depends on the sizes of the colliding particles x, y. We consider kernels $K = (xy)^\gamma$, but any homogeneous function can be treated using our methods. For sufficiently effective clumping $1 \geqslant \gamma > 1/2$, the coagulation equation produces an infinitely large cluster in finite time (a process known as the gel transition). Using a combination of analytical methods and numerics, we calculate the anomalous scaling dimensions of the main cluster growth. Apart from the solution branch which originates from the exactly solvable case $\gamma = 1$, we find a branch of solutions near $\gamma = 1/2$, which violates matching conditions for the limit of small cluster sizes, widely believed to hold on a universal basis.

DOI: 10.1103/PhysRevE.108.064110

I. INTRODUCTION

Smoluchowski's equation [1] has its origin in physical chemistry, but more generally furnishes a fundamental description of the formation of larger objects by the aggregation of smaller entities. It appears in many physical problems such as planetesimal accumulation, mergers in dense clusters of stars, aerosol coalescence in atmospheric physics, and polymerization and gelation (see [2–7]), but also in chemical engineering [7], and the social sciences [8,9] It describes the evolution of the density $c(x, t)$ of particles of size x at time t, taking into account the formation of clusters of size x by the aggregation of pairs of size $x - y$ and y, respectively, as well as the disappearance of clusters of size x forming a larger one:

$$c_t(x,t) = \frac{1}{2}\int_0^x K(x-y,y)c(x-y,t)c(y,t)dy - c(x,t)\int_0^\infty K(x,y)c(y,t)dy. \quad (1)$$

Here the function $K(x, y)$ (known as the coagulation kernel) describes the probability for two particles of sizes x and y to stick together.

The behavior of solutions to (1) depends crucially on the degree of homogeneity of K. To explore this, here we restrict ourselves to the class of models described by

$$K(x, y) = (xy)^\gamma, \quad (2)$$

for which the degree is 2γ. This kernel applies to branched polymers with surface interactions [4,10], and to fractal clusters more generally [11,12], but stands for a much broader class of models whose asymptotic behavior for large cluster sizes scales with an exponent 2γ. One of the fundamental problems in the field is to relate, by solving (1), γ to the scaling exponent $\sigma = \beta^{-1}$ determining the *typical* size of clusters, and the gel exponent τ, giving the power-law size distribution of clusters [4]. Thus by measuring β or τ, one is then able to infer fundamental mechanisms of aggregation, in phenomena as diverse as planetesimal formation [7], aerosol dynamics [13], or pipeline fouling caused by asphaltenes [14].

Only for $\gamma = 1$ can (1) be solved explicitly [15–18], for more general kernels studies have relied on discrete particle simulations and *ad hoc* scaling arguments (see [19] and references therein). It is therefore of enormous importance to develop mathematical methods able to provide novel information on the behavior of solutions to (1).

For $1/2 < \gamma \leqslant 1$, (1) develops singularities in finite time, such that, starting from an initial particle size distribution $c(x, 0)$ with all its moments $M_i = \int_0^\infty x^i c(x, 0)\, dx$ bounded, there is a certain time t_0 such that all moments M_i for $i \geqslant i_0$ diverge (see [20] and references therein). This phenomenon, which has the character of a phase transition [4], is called finite time gelation (at a gelation time t_0) and indicates the aggregation of particles in a single cluster of infinite mass. In practice, of course, the singularity will be cut off by the finite size of the total number of particles available, so that the largest clusters no longer grow. On the other hand, if $\gamma \leqslant 1/2$, solutions exist globally in time [21].

As in many other physical problems involving diverging quantities (cf. [4,22,23]), we assume that the approach to the

Published by the American Physical Society under the terms of the Creative Commons Attribution 4.0 International license. Further distribution of this work must maintain attribution to the author(s) and the published article's title, journal citation, and DOI.

singularity is self-similar, of the form

$$c(x,t) = t'^{\alpha}\psi(xt'^{\beta}); \tag{3}$$

here $t' = t_0 - t$ is the time distance to the singularity. We assume that the scaling function ψ is smooth, integrable, and positive, since $c(x,t)$ represents the density of particles.

The self-similar structure (3) has so far been established only for $\gamma = 1$, while for $\gamma < 1$ self-similar solutions have not been determined explicitly. Discrete numerical simulations (cf. [24,25]) appear to show *self-similarity of the second kind* [22], for which similarity exponents cannot be determined from dimensional considerations or from symmetry arguments. This fact was proven in [26] for $1-\gamma$ sufficiently small, without calculating the exponents explicitly.

Inserting the similarity form into (1) and balancing powers of t', one finds $\alpha - 1 = 2\alpha - (2\gamma+1)\beta$, and thus the scaling relation

$$\alpha = \beta(2\gamma+1) - 1. \tag{4}$$

It follows that

$$c(x,t) = t'^{\beta(2\gamma+1)-1}\psi(xt'^{\beta}), \tag{5}$$

the Laplace transform of which will form the basis of our analysis; the quantity $s(t) = \text{const}t'^{-\beta}$ is known as the typical cluster size [19]. In addition, one obtains an integral equation for the similarity profile $\psi(\xi)$; we will consider the Laplace transform of ψ below. The scaling form (5) is also known as the "self-preservation hypothesis" [3]; for example, using a rescaling analogous to (5), in Fig. 7.11 of [3] the distribution of aerosol particles, taken from experiment, is collapsed onto a single profile $\psi(\xi)$.

II. LAPLACE TRANSFORM METHOD

We begin by transforming (1) into Laplace space, always assuming a kernel of the form $K = (xy)^{\gamma}$. This equivalent formulation is more convenient then (1) for both numerical and analytical purposes, as we will see below. As the transformed variable we choose

$$\omega(\lambda,t) \equiv \int_0^\infty (1-e^{-\lambda x})xc(x,t)\,dx, \tag{6}$$

so that the total mass, which is conserved by (1), is

$$M_1 = \int_0^\infty xc(x,t)\,dx = \omega(\infty,t), \tag{7}$$

while $\omega(0,t) = 0$.

Multiplying (1) by $e^{-\lambda x}$ and integrating in x, the left-hand side becomes

$$\frac{\partial}{\partial t}\int_0^\infty e^{-\lambda x}c(x,t)\,dx, \tag{8}$$

while the first term on the right-hand side of (1) turns into

$$\begin{aligned}&\int_0^\infty e^{-\lambda x}\left[\frac{1}{2}\int_0^x x^{\gamma}(x-y)^{\gamma}c(x-y,t)c(y,t)\,dy\right]dx\\ &= \frac{1}{2}\int_0^\infty\int_0^\infty e^{-\lambda(z+y)}y^{\gamma}z^{\gamma}c(z,t)c(y,t)\,dy\,dz\\ &= \frac{1}{2}\left[\int_0^\infty e^{-\lambda x}x^{\gamma}c(x,t)\,dx\right]^2,\end{aligned}$$

while the second term becomes

$$-\left[\int_0^\infty e^{-\lambda x}x^{\gamma}c(x,t)\right]\int_0^\infty x^{\gamma}c(x,t).$$

Taken together, we can write the right-hand side as

$$\frac{1}{2}\left[\int_0^\infty (e^{-\lambda x}-1)x^{\gamma}c(x,t)\,dx\right]^2 - \frac{1}{2}\left[\int_0^\infty x^{\gamma}c(x,t)\right]^2. \tag{9}$$

To transform this into a closed equation for ω, we take the λ derivative of both (8) and (9) and use mass conservation, $\partial_t M_1 = 0$, to find

$$\frac{\partial\omega}{\partial t} = \frac{1}{2}\frac{\partial}{\partial\lambda}\left[\int_0^\infty (1-e^{-\lambda x})x^{\gamma}c(x,t)\,dx\right]^2. \tag{10}$$

The right-hand side of (10) can be rewritten using

$$\begin{aligned}&\frac{1}{\Gamma(1-\gamma)}\int_0^\infty \frac{\omega(\lambda+y,t)-\omega(y,t)}{y^{\gamma}}\,dy\\ &= \frac{1}{\Gamma(1-\gamma)}\int_0^\infty \frac{1}{y^{\gamma}}\left[\int_0^\infty (e^{-yx}-e^{-(\lambda+y)x})xc(x,t),dx\right]dy\\ &= \frac{1}{\Gamma(1-\gamma)}\int_0^\infty \left[\int_0^\infty e^{-yx}y^{-\gamma}\,dy\right]\left(1-e^{-\lambda x}\right)xc(x,t)\,dx\\ &= \int_0^\infty (1-e^{-\lambda x})x^{\gamma}c(x,t)\,dx,\end{aligned}$$

so that we finally obtain

$$\frac{\partial\omega}{\partial t}(\lambda,t) = \frac{1}{2}\frac{\partial}{\partial\lambda}\left[\int_0^\infty \frac{\omega(\lambda+\zeta,t)-\omega(\zeta,t)}{\Gamma(1-\gamma)\zeta^{\gamma}}\,d\zeta\right]^2, \tag{11}$$

which we will consider for the remainder of this paper.

The Laplace formulation (11) is similar to the nonlinear transport equations investigated by us previously [27] and for whose solution we have developed efficient numerical methods. For $\gamma = 1$, the expression in square brackets is $\omega(\lambda,t)$, so that (11) turns into Burgers' equation. If $\gamma < 1$, one can think of (11) as a generalization of Burgers' equation, but with ordinary derivatives replaced by fractional derivatives. In a later section, we will simulate the time-dependent equation (11) directly, but first we consider similarity solutions to determine the blow up of cluster sizes.

Similarity solutions

Using (4), we now look for similarity solutions of (11), defined by

$$\omega(\lambda,t) = t'^{\beta(2\gamma-1)-1}\beta\Phi(\eta), \quad \eta = \lambda/t'^{\beta}, \tag{12}$$

which is consistent with (5); the factor β was introduced for later convenience. Of course, $\Phi(\eta)$ is related to $\psi(\xi)$ by Laplace transform [26]:

$$\Phi(\eta) = \frac{1}{\beta}\int_0^\infty (1-e^{-\eta\xi})\xi\psi(\xi)\,d\xi. \tag{13}$$

The behavior of $\Phi(\eta)$ for large arguments represents the distribution of small clusters; if $\psi(\xi) \propto \xi^{-\tau}$ for $\xi \to 0$ (see (3.19) of [19]), then $\Phi(\eta) \propto \eta^{\tau-2}$ for $\eta \to \infty$, where τ is known as the (pre)gel exponent [28]. This implies that as t_0 is approached, the distribution function for small clusters approaches a power law $c(x,t_0) \propto x^{-\tau}$, which will once more

link to the kernel's exponent γ. Similar power-law distributions occur in many other fields, such as Zipf's law [8], and have been proposed to understand phenomena such as bank mergers [9].

Inserting (12) into (11), we recover the scaling relation (4) from a balance of both sides. Dividing through by β, we have

$$-\nu\Phi(\eta)+\eta\Phi'(\eta)=\frac{1}{2}\frac{dF^2}{d\eta}, \tag{14}$$

with F defined by

$$F\equiv\frac{1}{\Gamma(1-\gamma)}\int_0^\infty\frac{\Phi(\eta+\zeta)-\Phi(\zeta)}{\zeta^\gamma}d\zeta, \tag{15}$$

and $\nu=(2\gamma-1)\beta-1)/\beta$. It is advantageous to eliminate β from the equation in favor of ν, since β diverges as γ approaches 1/2, while ν remains finite. Similarity equations similar to (14) have been considered previously by [19,26].

The left-hand side of (14) corresponds to the time derivative of the Smoluchowski equation, which is expected to vanish for large η in order for the solution to match to the "background" of the distribution of small clusters. This matching condition [23] then implies that $\Phi(\eta)\propto\eta^\nu$ for large η, which according to the above leads to the scaling relation $\tau=2+\nu=1+2\gamma-\sigma$ [19], which relates the gel exponent τ with the exponent $\sigma\equiv\beta^{-1}$, determining the typical cluster size. In summary,

$$\tau=2+\nu,\quad \sigma=2\gamma-\nu-1 \tag{16}$$

can be used to recover physically significant exponents from ν. We will see below that the matching condition leading to (16) holds true only for the "lower" branch of solutions, which grows out of the classical case $\gamma=1$, but fails for the "upper" branch, reported here.

III. THE LOWER BRANCH

We are looking for solutions to (14) with $\Phi(\eta)$ regular at the origin and $\Phi(\eta)\approx A\eta^\nu$ for $\eta\to\infty$, where A is a constant to be found as part of the solution, along with ν. In the exactly solvable case $\gamma=1$, we have $F=\Phi(\eta)$, so (14) becomes

$$-\nu\Phi+\eta\Phi'=\Phi\Phi', \tag{17}$$

the same as for the kinematic wave equation [26,30]. This equation has an infinite sequence of regular solutions

$$\eta=\frac{1+j}{j}\Phi+B\Phi^{1+j},\quad j=1,2,\ldots, \tag{18}$$

where B is an arbitrary constant. For the "ground" state $j=1$, the cluster size exponent is $\beta=2$, and $\nu=1/2$. A sequence of nontrivial solution branches, exhibiting anomalous scaling exponents, emanate from each of these exact solutions; we will focus on the ground-state branch, which is expected to be attracting, while all other branches are unstable.

To evaluate faithfully the contributions to the improper integral in (15), it is useful to have a good approximation of $\Phi(\eta)$ for large arguments, beyond the leading order matching condition $\Phi(\eta)\approx A\eta^\nu$. Perturbing around this asymptotic behavior, we find that to leading order

$$\begin{aligned}F&\approx\frac{A}{\Gamma(1-\gamma)}\int_0^\infty\frac{(\eta+\zeta)^\nu-\zeta^\nu}{\zeta^\gamma}d\zeta\\&=\frac{A\eta^{\nu-\gamma+1}}{\Gamma(1-\gamma)}\int_0^\infty\frac{(1+z)^\nu-z^\nu}{z^\gamma}dz=AC_\nu\eta^{\nu-\gamma+1},\end{aligned}$$

where

$$C_\nu\equiv\frac{\Gamma(\gamma-1-\nu)}{\Gamma(-\nu)}. \tag{19}$$

Inserting this back into the right-hand side of (14), one finds that Φ has the expansion

$$\Phi\approx A\eta^\nu+A^2C_\nu^2\frac{1+\nu-\gamma}{1+\nu-2\gamma}\eta^{1-2\gamma+2\nu}+\cdots \tag{20}$$

for large η.

The numerical procedure used to solve (14) is similar to that developed in [27] to solve nonlocal transport equations. The function Φ is discretized on a grid η_i, $i=1,\ldots,k$, where $\eta_1=0$ and $\Phi_i=\Phi(\eta_i)$. We use local refinement near the origin, based on the width of the peak of Φ', which sets the scale over which the solution is varying. To resolve the tip of the distribution Φ, the grid spacing is at first constant near the origin. Then, in order to resolve the distribution over many orders of magnitude (up to 70 orders of magnitude in some cases, as seen below), we allow the grid spacing to increases geometrically up to a large value η_k. Beyond η_k, we use the asymptotic expansion (20), in which A is treated as an unknown, which is solved for, as described below. For each case, we made sure that the result did not depend on a particular choice of the parameters characterizing the discretization.

In order to evaluate the improper integral in (15), we split the domain of integration into the interval $[0,\eta_k]$ and the remainder (η_k,∞). In the first integral, we use a formula equivalent to the trapezoidal rule, but taking into account the singularity at the origin explicitly; the value of $\Phi(\eta+\zeta)$ is found by interpolating from the fixed grid. If the argument $\eta+\zeta$ of Φ is greater than η_k, we use the asymptotic expansion (20) to evaluate Φ. For the second integral, in which $\zeta>\eta_k$, we use (20) everywhere, and then evaluate the integral numerically.

We will see below that for γ near 1/2, Φ has a complicated crossover behavior, so that (20) becomes valid only for very large values of η; thus one has to choose η_k large enough for (20) to be meaningful. Depending on γ, we allow η_k to be as large as $10^{70}\approx e^{161}$, verifying that the result does not depend significantly on the choice of η_k.

The similarity equation (14) is invariant under the transformation

$$\Phi(\eta)=a\varphi(\eta/a^{1/(2\gamma-1)}); \tag{21}$$

to fix the constant a, we impose $\Phi'(0)$. It is easy to check that the ground-state solution for $\gamma=1$ always satisfies $\Phi'(0)=1/2$, so we impose this condition for arbitrary γ, in order to find a unique solution. It is clear from (13) that we also have to impose $\Phi(0)=0$.

This reduces the lower branch problem to a system of nonlinear equations defined on the grid η_i, where the k variables are the index ν, the amplitude A, and the values Φ_i, $i=$

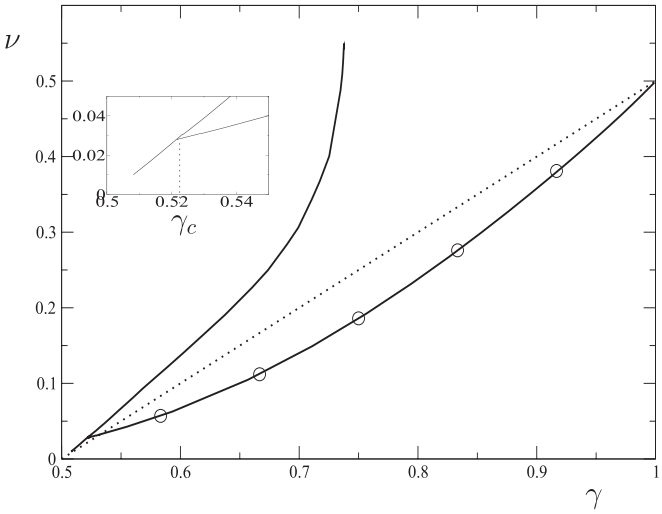

FIG. 1. The exponent ν for γ between 1/2 and 1. One branch (the lower branch) starts from $\gamma = 1$, $\nu = 1/2$ on the right and ends by intersecting another branch (the upper branch) at $\gamma_c \approx 0.5214$. The scaling $\nu = \gamma - 1/2$ [19] is shown as the dotted line. The inset shows a detail of the bifurcation, where the two branches meet at γ_c. The circles mark the result of particle-based simulations of Lee [25]. In [29], exponents are calculated solving the similarity equation directly, but only for $\gamma = 3/4$, for which the result agrees with [25].

$2, \ldots, k-1$ of the profile. The equations are $\Phi'(0) = 1/2$ and (14), evaluated at η_i, $i = 2, \ldots, k$. This system of equations is solved using Newton's method, using $\eta_k = 10^{10}$ up to $\gamma \approx 0.53$; for smaller γ, the solution is extended to $\eta_k \approx 10^{70}$. To obtain a good initial guess, we start from the "ground-state" solution for $\gamma = 1$ as an initial condition, and continue the solution branch in small steps of γ. The Newton iteration eventually fails to converge for $\gamma \approx 0.5217$, indicating a bifurcation toward the upper branch. For higher order branches we once again start from the exact solution for $\gamma = 1$, but choosing $j > 1$. In this case $\Phi'(0) = j/(1+j)$, which we use as the normalization for all values of γ.

The resulting values of ν, which make up the "lower branch," are shown in Fig. 1 as the lower solid line, emanating from $\nu = 1/2$ for $\gamma = 1$. Starting from the exact solution for $\gamma = 1$, a solution is found by proceeding in small steps of γ, the preceding solution being used as an initial condition. A typical profile $\Phi(\eta)$, for the intermediate value $\gamma = 0.794$, is shown as the dotted line in the inset of Fig. 4 below. The solid line comes from solving the dynamical equation (11) directly.

In a number of papers [10,28,31–33], it was proposed (see also the discussion in Sec. 3.5.4 of [19]) that scaling relations might be derived from the condition that the rate of change of the total mass M_1 should remain finite. While this is certainly true after the gel time, it does not necessarily hold for our case, and indeed is erroneous, as seen below. However, making this assumption for the time being, this means that dM_1/dt remains bounded. Using the similarity form (5), this implies that $t'^{\beta(2\gamma+1)-1} \sim t'$, or $\beta = 2/(2\gamma-1)$. It follows that $\nu = ((2\gamma-1)\beta - 1)/\beta = \gamma - 1/2$, and also $\sigma = (2\gamma-1)/2$. The scaling relation $\nu = \gamma - 1/2$ is shown as the dotted line in Fig. 1, clearly in strong disagreement with the actual solution of (14). This confirms the numerical results of Lee [25], obtained using a particle-based description, which are discussed in detail in [19] and which are shown as circles in Fig. 1. The same conclusions were reached rigorously [26], by investigating the neighborhood of the exact solution for $\gamma = 1$. Indeed, in (14) the behaviors for small and for large clusters are in fact coupled, which leads to *anomalous* scaling exponents [22,23], invalidating a simple linear scaling.

To summarize our numerical results so far, we developed an interpolation formula, which describes the lower solution branch to three decimal places, where $\varepsilon \equiv 1 - \gamma$:

$$\nu = \tfrac{1}{2} - \tfrac{3}{2}\varepsilon + 1.1044\varepsilon^2 \log\varepsilon + 3.8187\varepsilon^2 - 6.4849\varepsilon^3 + 5.14\varepsilon^4. \tag{22}$$

Extending the result of [26] for small ε, we fitted the lower branch data using a least squares approach. The coefficient of ε was chosen in accordance with the slope $d\nu/d\gamma = 3/2$ for $\gamma = 1$, which was proved in [26]. The logarithm was also suggested by the analysis of [26] and yields a significantly improved fit.

We have also calculated solution branches which emanate from the higher-order solutions at $\gamma = 1$, which are known to be unstable [23]. It is therefore likely that the entire higher-order branches are unstable. Indeed, we have also solved the time-dependent evolution equations in Laplace space for the particular value of $\gamma = 0.7942$, and found the solution to converge onto the stable ground-state solution, shown in Fig. 1; see Sec. V below.

Transition toward the upper branch

As γ decreases toward 1/2, the correction exponent $1 - 2\gamma + 2\nu$ in (20) becomes ever closer to ν, so a larger domain is needed to correctly describe the asymptotics for large η, as seen in Fig. 2. In this case we have chosen $\eta_k \approx e^{161}$, beyond which value the dashed line, representing (20), is a good approximation to the solid line (the full solution). The two exponents become identical for $\nu = 2\gamma - 1 \equiv \delta$, which suggests the appearance of an alternative branch of solutions, for which $\Phi(\eta) \sim \eta^\delta$, and which we call the "upper branch," also shown in Fig. 1. This transition occurs at $\gamma \approx 0.5214$, close to the critical value of $\gamma = 1/2$, in a regime that has not been explored previously; the smallest value considered in [25] is $\gamma = 7/12 \approx 0.58$.

To understand the transition between the two branches, we write a formal solution of the similarity equation (14):

$$\Phi(\eta) = \frac{F^2}{2\eta} + \frac{1+\nu}{2}\eta^\nu \int_0^\eta \frac{F^2}{\eta^{2+\nu}}\, d\eta. \tag{23}$$

If the integral in (23) is convergent, then the second term scales like η^ν, and

$$A = \frac{1+\nu}{2}\int_0^\infty \frac{F^2(\eta')}{\eta'^{2+\nu}}\, d\eta'; \tag{24}$$

the first term in (23) is seen to be subdominant.

We anticipate a nonuniform convergence of the lower branch toward the upper branch as $\gamma \to \gamma_c$. Let us assume that as suggested by Fig. 2, for $1 \lesssim \eta \lesssim \eta_c$, $\Phi \sim \eta^\delta$, while for $\eta_c \lesssim \eta \lesssim \infty$, $\Phi \sim \eta^\nu$. Since the integral in (24) converges

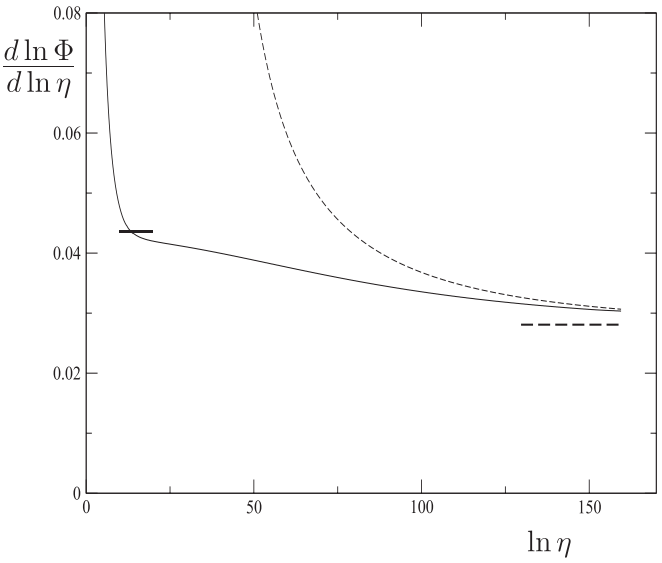

FIG. 2. The local exponent of $\Phi(\eta)$ over a large domain, with $\gamma = 0.521829$. In performing the integral in (15), for arguments $\eta < \eta_k = 10^{70} \approx e^{161}$, $\Phi(\eta)$ is being used as shown. For arguments $\eta > \eta_k$, this is replaced by the approximation (20). The solid line is the full solution on the lower branch, the dashed line is (20). The solid horizontal line on the left is $\delta = 2\gamma - 1 = 0.04366$, the dashed horizontal line on the right is $\nu = 0.02808$.

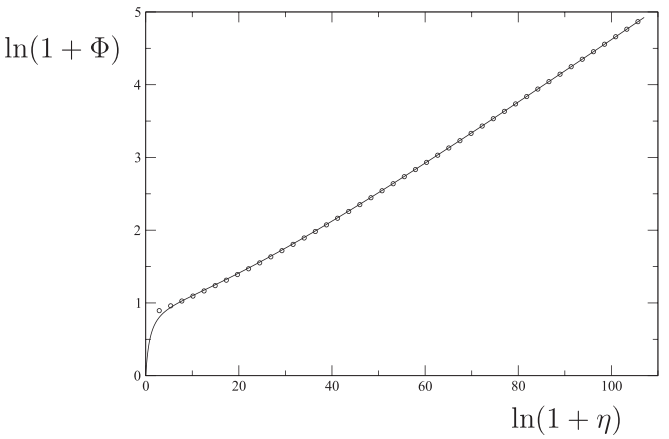

FIG. 3. The profile $\Phi(\eta)$ on the upper branch, on a double logarithmic scale (solid line), compared to the asymptotics (25) (circles); $\gamma = 0.521829$, the same as in Fig. 2, and $\nu = 0.0285$.

for $\Phi \sim \eta^{\nu}$, this means that $A \sim \eta_c^{\delta-\nu}$, where the exponent is positive on the lower branch, so that as $\eta_c \to \infty$, the prefactor A diverges. Indeed, a best fit to the numerical data yields $A \approx A_0/(\gamma - 0.521)^{\bar{\beta}}$, with $\bar{\beta} = 0.348$ and $A_0 = 0.44$, a blowup at γ very close to the extrapolated value of $\gamma = \gamma_c = 0.5214$.

If on the other hand the integral in (23) is divergent, both terms on the right of (23) scale in the same way. Then using the ansatz $\Phi \approx \bar{A}\eta^{\delta}$, we can calculate the asymptotic behavior of F as $F \approx \bar{A}C_{\delta}\eta^{\delta+1-\gamma}$. Inserting this into (23), and balancing both sides yields

$$\Phi \approx \frac{\delta - \nu}{\gamma C_{\delta}^2}\eta^{2\gamma-1} \equiv \bar{A}\eta^{\delta}, \tag{25}$$

to leading order as $\eta \to \infty$.

IV. THE UPPER BRANCH

To evaluate the integral in (15) along the upper branch, for $\eta \geqslant \eta_k$ we now use (25) instead of (20). Note that according to (25), the amplitude $\bar{A}$ is no longer an unknown, but can be calculated in terms of ν and $\delta = 2\gamma - 1$.

To account for the scale invariance (21) of Φ, we impose $\Phi'(0) = 1$. The variables are now ν and Φ_i, $i = 2, \ldots, k-1$. In order to suppress oscillations in $\Phi(\eta)$, which appear for large values of η, we found it necessary to solve *the first derivative of* (14) (as we did before in [27]). Imposing this condition at infinity, we were able to nucleate an upper branch solution from the lower branch, using a γ close to the bifurcation. The branch is then continued to the left and to the right.

A typical profile on the upper branch is shown in Fig. 3, using a logarithmic scale, except near the origin. The dashed line is the expected asymptotics (25), and γ is the same as in Fig. 2, showing the lower branch. This demonstrates that for a range of γ values above γ_c, there are multiple solutions. This is also clear from the phase diagram in Fig. 1, where both branches are shown. The lower branch ends at γ_c, where it meets the upper branch, as seen in the inset. There appears to be unique asymptotic behavior coming in for $\gamma \lesssim 1/2$, which makes it difficult to continue the upper branch all the way to $\gamma = 1/2$.

An interesting feature of the upper branch is that $\eta^{\nu} \equiv \eta^{\alpha/\beta-2}$ does not equal the true asymptotic behavior $\Phi \approx \bar{A}\eta^{\delta}$, which is represented by circles in Fig. 3. As a result, the Laplace transform $\omega(\lambda, t)$ of the cluster size distribution on account of (12) behaves for large arguments like $\omega(\lambda, t) \approx \beta\bar{A}\lambda^{\delta}t'^{-1}$, which for $t' \to 0$ diverges, and hence does not match the expected static distribution at large arguments.

This implies that for the upper branch there must be another, *outer* region, which interpolates between the asymptotics (25) and a time-independent outer solution. This is described by an outer similarity solution, which we present now.

Outer solution

The outer solution

$$\omega(\lambda, t) = t'^{\bar{\lambda}}\varphi(\zeta), \quad \zeta = \lambda t'^{-(1+\bar{\lambda})/\delta} \tag{26}$$

succeeds in bridging the time dependence $\omega \propto t'^{-1}$ with a static outer distribution, as we will now show; $\bar{\lambda}$ is another anomalous exponent to be determined. Inserting (26) into (11) yields the similarity equation

$$-\bar{\lambda}\varphi + \frac{1+\bar{\lambda}}{\delta}\zeta\varphi' = F^{(\varphi)}\frac{dF^{(\varphi)}}{d\zeta}, \tag{27}$$

where $F^{(\varphi)}$ is the same as (15), but with Φ replaced by φ. Equation (27) has a solution $\zeta^{\delta}/(\gamma C_{\delta}) = \beta\bar{A}\zeta^{\delta}$, which for $\zeta \to 0$ matches the asymptotics (25) of the upper branch.

To understand the consistency of the behavior for small ζ, we look for solutions to (27) of the form

$$\varphi \approx \beta\bar{A}\zeta^{\delta} + g(\zeta).$$

Linearizing in g, we arrive at

$$-\bar{\lambda}g + \frac{1+\bar{\lambda}}{\delta}\zeta g' = \frac{d}{d\zeta}\left(\frac{2\zeta^{(1+\delta)/2}}{(1+\delta)C_\delta}F^{(g)}\right),$$

which has a solution of the form $g(\zeta) = G\zeta^{\bar{\alpha}}$, where $\bar{\alpha}$ satisfies

$$\left(\frac{1+\bar{\lambda}}{\delta} - \bar{\lambda}\right)\bar{\alpha} = \frac{2(1+\bar{\alpha})C_{\bar{\alpha}}}{(1+\delta)C_\delta}. \tag{28}$$

For small $\delta, \bar{\lambda}$, (28) simplifies to

$$2(1+\bar{\alpha})\Gamma(1/2-\bar{\alpha}) = (1+2\bar{\alpha})\Gamma(1-\bar{\alpha})\sqrt{\pi},$$

whose dominant (smallest) solution is $\bar{\alpha} = \alpha_0 = 1.30737\ldots$.

In the limit of large ζ, on the other hand, the time dependence of (26) must drop out, so we have to require that $\varphi(\zeta) \approx \varphi_0\zeta^{\bar{\lambda}\delta/(1+\bar{\lambda})}$. This will ensure that for small cluster sizes, ω matches onto a static cluster size distribution. The exponent $\bar{\lambda}$ plays the role of a nonlinear eigenvalue, with the constant G in $g(\zeta)$ providing a shooting parameter, which is adjusted such that φ has the right power-law behavior at infinity.

While the existence of an outer solution is relevant for the consistency of the outer solution, its exact form is not important for the rate of blow up of moments

$$M_i = \int_0^\infty x^i c(x,t)\,dx, \tag{29}$$

as found on the upper branch. As a result, all moments can be computed in terms of derivatives of the Laplace transform, evaluated at the origin. For example, according to (6) the second moment is

$$M_2 = \frac{\partial\omega}{\partial\lambda}(0,t) = t'^{2\beta(\gamma-1)-1}\beta\Phi'(0),$$

where $\beta = 1/(\delta-\nu)$. But $\Phi'(0)$ can be found from the profile $\Phi(\eta)$ (cf. Fig. 3), as computed as part of the solution of the upper branch, without knowledge of the outer solution.

V. DYNAMICAL SIMULATIONS

As a further test of the validity of the similarity solutions obtained so far, here we integrate the Laplace-transformed dynamical equations directly, as given by (11). As a first example, we choose $\gamma = 0.794$, in the range $1/2 < \gamma \leqslant 1$, for which finite time blowup is observed. This demonstrates the stability of the similarity solution obtained previously. Second, we look at $\gamma = 1/4$, from a range of values for which blowup occurs in infinite time only. In both cases, we use the initial condition

$$\omega(\lambda,0) = 1 - e^{\lambda/(\lambda-1)}, \tag{30}$$

which approaches the limiting value of 1 to all orders, as $\lambda \to 1$. As a result, the integral on the right-hand side of (11) has to be evaluated only up to $\zeta = 1$, since the integrand vanishes for the remainder. In time, the condition $\omega(1,t) = 1$ continues to hold, so that the boundary condition $\omega(\infty,t) = 1$ remains satisfied, which implies mass conservation. Otherwise, the integral on the right-hand side of (11) is evaluated in the same way as described before in the case of the similarity equation (14).

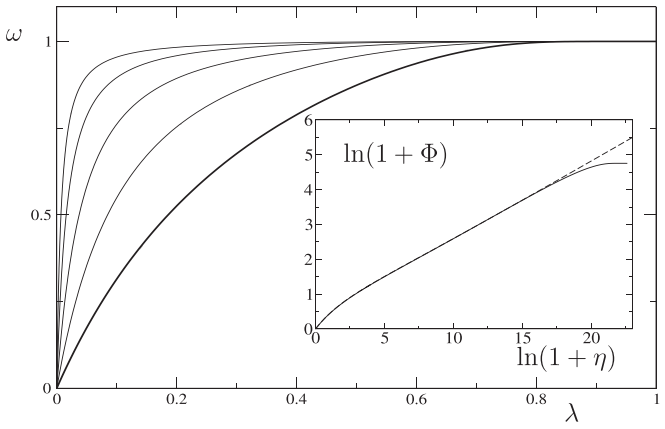

FIG. 4. Comparison of similarity theory with direct numerical simulation of (11) for $\gamma = 0.794$. In the main panel, a sequence of profiles as obtained from (11); the heavy line is the initial condition. As the inset, the last profile $\omega(\lambda,t)$ is rescaled using the exponents obtained from solving (14): $\nu = 0.2277$, so that $\beta = 2.773$ (solid line). The dashed line is the similarity profile $\Phi(\eta)$, which is a solution of (14); scales are logarithmic.

The time step is performed explicitly, combining a full time step and two half steps to achieve second-order accuracy. The difference between the two is used as an error control, to choose the time step [23]. The resulting sequence of profiles is shown in the main panel of Fig. 4, starting from (30) (heavy line). The profile propagates to the left, producing an increasingly sharp front. Simulations are continued until the width of the front, as defined by the position of the maximum of the right-hand side of (11), falls below 10^{-9}.

In the inset of (4) we show the last profile, rescaled according to (12), in order to obtain an approximation to $\Phi(\eta)$ (solid line). The invariance (21) of the profile is used to impose $\Phi'(0) = 1/2$ at the origin. A solution to the similarity equation (14) is superimposed (dashed line), and almost perfect agreement is found. Notice, however, that the rescaled solution of (11) levels off at a certain point, as it must to satisfy $\omega(\infty,t) = 1$ for all times, reflecting mass conservation. The similarity solution, on the other hand, corresponds to a cluster distribution which does not have a first moment. This illustrates how a solution with finite, conserved mass nevertheless approximates the similarity solution in a nonuniform fashion.

If on the other hand $0 < \gamma < 1/2$, mass is conserved for all times, and the cluster size diverges in infinite time only. The similarity form of the cluster size distribution is now [4,34]

$$c(x,t) = t^\alpha\psi(xt^\beta), \tag{31}$$

so that mass conservation implies

$$M_1 = t^{\alpha-2\beta}\int_0^\infty \xi\psi(\xi)\,d\xi$$

finite, and $\alpha = 2\beta$. Together with (4) we obtain the scaling relation $\beta = 1/(2\gamma-1)$, which should be valid for $\gamma < 1/2$. To test this, we performed time-dependent simulations of (11) for $\gamma = 1/4$. Since (12) now takes the form

$$\omega(\lambda,t) = t^{\alpha-2\beta}\beta\Phi(\lambda t^{-\beta}),$$

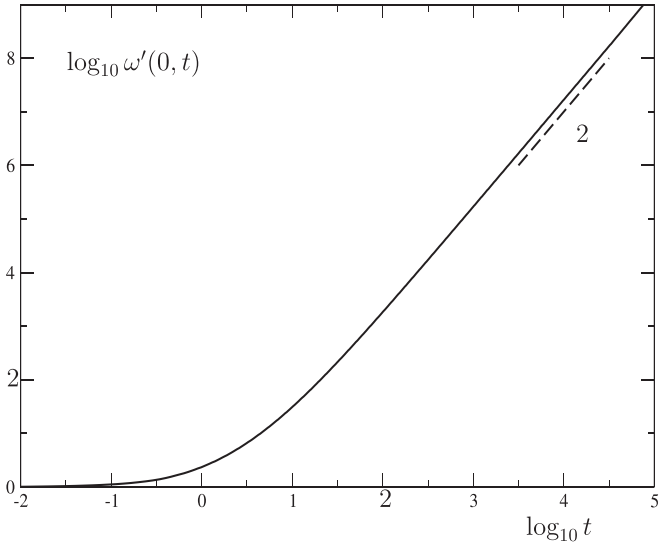

FIG. 5. Scaling of cluster size for $\gamma = 1/4$ (infinite time singularity). The solid line shows $\partial_\lambda \omega(0,t)$ as a function of t in a double logarithmic plot. Mass conservation predicts an exponent of $1/(1-2\gamma) = 2$ in that case (dashed line), in very good agreement with our numerics.

the slope at the origin should scale like

$$\frac{\partial \omega}{\partial \lambda} \propto t^{\alpha-3\beta} \propto t^{-\beta} \propto t^{1/(2\gamma-1)}.$$

In Fig. 5 we have plotted this quantity as a function of time. For large times, we find very good agreement with the prediction $1/(2\gamma-1) = 2$, expected for $\gamma = 1/4$, in agreement with earlier conclusions by Lee [25].

Finally, we have also performed simulations for γ around the critical value γ_c, in order to confirm that the upper branch is indeed stable for $1/2 < \gamma < \gamma_c$. However, owing to the smallness of the relevant values of ν, our resolution is not sufficient to reach any firm conclusions.

VI. DISCUSSION

Our numerical simulations of the dynamical equations demonstrate the stability and the physical realizability of the solution branches we have found, at least for some values of γ. However, mathematical issues remain in relation to the solution branches over the full range $1/2 < \gamma \leqslant 1$. First, although we find self-similar solutions which satisfy the correct asymptotics, it is not clear if they are stable, at least linearly. Second, a problem with the Laplace transform method we used is that the original scaling function $\psi(\xi)$ is not automatically positive, as required for a physical solution. For the lower branch in the neighborhood of $\gamma = 1$, positivity was proved in [26]. Apart from this, both the stability and positivity remain open problems for general γ.

There are many directions in which to extend the present research. First, it would be interesting to consider (1) for times after the singularity and establish postgel solutions, including the scaling relations they satisfy. Second, we have not been able to extend the upper solution branch to the limiting case $\gamma = 1/2$. We have found a solution to (14) with $\nu = 0$, which is of the form

$$\omega(\lambda, t) = \Phi(\lambda e^t), \quad \eta = \lambda e^t, \tag{32}$$

which would imply that $s(t) = \exp(\text{const}\, t)$. On the other hand, Lee [25] has compared (32) to the alternative scaling $s(t) \propto \exp(\text{const}\sqrt{t})$, proposed in [33], and concluded that the latter scaling provides a better fit. However, we believe that owing to the limited range over which scaling was observed, it is difficult to draw definitive conclusions even from the high resolution data of [25]. Unfortunately, our own dynamical simulations are not sufficiently accurate to distinguish between the two scenarios.

Third, many studies have looked at other types of homogeneous kernels [4], such as $K = x^\lambda y^\nu$ or $K = x^\lambda + y^\lambda$. For example, an important question is whether exponents depend only on the degree of homogeneity $\lambda = \mu + \nu$, or whether they are more sensitive to the structure of the kernel. Indeed, our methodology extends to much more general kernels, for example, of the form $K(x,y) = (x^\mu y^\nu + x^\nu y^\mu)/2$ (with $\mu + \nu = 2\gamma$). This would lead to the integro-differential equation (14), with the right-hand side replaced by $\frac{1}{2}\frac{d(F_\mu F_\nu)}{d\eta}$, where F_μ and F_ν are defined as in (15), with γ replaced by μ and ν, respectively.

In wave turbulence [35–38], similar integral equations arise, which have not been solved explicitly, as we do here. Instead, the theory rests on scaling assumptions similar to those which in coagulation theory were found to be invalid. Here a stationary turbulent spectrum would correspond to postgel solutions, which evolve out of the initial singularity; see, for example, [38], Sec. 9.2.3. It is therefore possible that a more careful treatment of the integral equations of wave turbulence yields anomalous dimensions, as has been conjectured [37], which would change the scaling exponents of (say) the velocity field of the turbulence. Similar issues arise in Bose-Einstein condensation, where numerical results point to anomalous scaling exponents different from the classical ones [39–41].

In conclusion, integro-differential equations represent an area where some of today's most challenging unsolved problems in statistical mechanics and in fluid dynamics come together. Using self-similar solutions to the Smoluchowski equation, we showed that such integral equations have many unexpected properties, which challenge long-held beliefs.

[1] M. von Smoluchowski, Drei Vorträge über Diffusion, Brownsche Molekularbewegung und Koagulation von Kolloidteilchen, Phys. Z. **17**, 585 (1916).

[2] R. L. Drake, A general mathematical survey of the coagulation equation, in *Topics in Current Aerosol Research (Part 2)*, edited by G. M. Hidy and J. R. Brock (Pergamon, Oxford, 1972), pp. 201–376.

[3] S. K. Friedlander, *Smoke, Dust and Haze* (Oxford University Press, Oxford, 2000).

[4] M. H. Ernst, Kinetics of clustering in irreversible aggregation,

in *Fractals in Physics*, edited by L. Pietronero and E. Tosatti (North-Holland, Amsterdam, 1986), pp. 289–302.
[5] R. Jullien and R. Botet, *Aggregation and Fractal Aggregates* (World Scientific, Singapore, 1987).
[6] M. H. Lee, *N*-body evolution of dense clusters of compact stars, Astrophys. J. **418**, 147 (1993).
[7] P. Garaud, F. Meru, M. Galvagni, and C. Olczak, From dust to planetesimals: An improved model for collisional growth in protoplanetary disks, Astrophys. J. **764**, 146 (2013).
[8] X. Gavaix, Power laws in economics: An introduction, J. Econ. Perspect. **30**, 185 (2016).
[9] Z. Banakar, M. Tavana, B. Huff, and D. Di Caprio, A bank merger predictive model using the Smoluchowski stochastic coagulation equation and reverse engineering, Int. J. Bank Market. **36**, 634 (2018).
[10] E. M. Hendriks, M. H. Ernst, and R. M. Ziff, Coagulation equations with gelation, J. Stat. Phys. **31**, 519 (1983).
[11] P. Meakin, Formation of fractal clusters and networks by irreversible diffusion-limited aggregation, Phys. Rev. Lett. **51**, 1119 (1983).
[12] M. Kolb, R. Botet, and R. Jullien, Scaling of kinetically growing clusters, Phys. Rev. Lett. **51**, 1123 (1983).
[13] S. K. Friedlander and C. S. Wang, The self-preserving particle size distribution for coagulation by Brownian motion, J. Coll. Int. Sci. **22**, 126 (1966).
[14] C. V. B. Fávero, T. Maqbool, M. Hoepfner, N. Haji-Akbari, and H. S. Fogler, Revisiting the flocculation kinetics of destabilized asphaltenes, Adv Coll. Int. Sci. **244**, 267 (2017).
[15] G. Menon and R. L. Pego, Dynamical scaling in Smoluchowski's coagulation equations: Uniform convergence, SIAM Rev. **48**, 745 (2006).
[16] G. Menon and R. L. Pego, The scaling attractor and ultimate dynamics for Smoluchowski's coagulation equations, J. Nonlinear Sci. **18**, 143 (2008).
[17] M. Escobedo and J. J. L. Velázquez, On the fundamental solution of a linearized homogeneous coagulation equation, Commun. Math. Phys. **297**, 759 (2010).
[18] M. Herrmann, P. Laurençot, and B. Niethammer, Self-similar solutions for fat tails for a coagulation equation with nonlocal drift, C. R. Math. Acad. Sci. Paris **347**, 909 (2009).
[19] F. Leyvraz, Scaling theory and exactly solved models in the kinetics of irreversible aggregation, Phys. Rep. **383**, 95 (2003).
[20] M. Escobedo, S. Mischler, and B. Perthame, Gelation in coagulation and fragmentation models, Commun. Math. Phys. **231**, 157 (2002).
[21] M. Escobedo and S. Mischler, Dust and self-similarity for the Smoluchowski coagulation equation, Ann. Inst. Henri Poincaré **23**, 331 (2006).
[22] G. I. Barenblatt, *Similarity Self-Similarity and Intermedeate Asymptotics* (Cambridge University Press, Cambridge, 1996).
[23] J. Eggers and M. A. Fontelos, *Singularities: Formation, Structure, and Propagation* (Cambridge University Press, Cambridge, 2015).
[24] G. Menon and R. L. Pego, Approach to self-similarity in Smoluchowski's coagulation equations, Commun. Pure Appl. Math. **57**, 1197 (2004).
[25] M. H. Lee, A survey of numerical solutions to the coagulation equation, J. Phys. A **34**, 10219 (2001).
[26] G. Breschi and M. A. Fontelos, Self-similar solutions of the second kind representing gelation in finite time for the Smoluchowski equation, Nonlinearity **27**, 1709 (2014).
[27] J. Eggers and M. A. Fontelos, Selection of singular solutions in non-local transport equations, Nonlinearity **33**, 325 (2020).
[28] P. G. J. van Dongen and M. H. Ernst, Dynamic scaling in the kinetics of clustering, Phys. Rev. Lett. **54**, 1396 (1985).
[29] F. Leyvraz, Scaling theory for gelling systems: Work in progress, Physica D **222**, 21 (2006).
[30] J. Eggers and M. A. Fontelos, The role of self-similarity in singularities of partial differential equations, Nonlinearity **22**, R1 (2009).
[31] E. M. Hendriks, M. H. Ernst, and R. M. Ziff, Kinetics of gelation and universality, J. Phys. A: Math. Gen. **16**, 2293 (1983).
[32] F. Leyvraz and H. R. Tschudi, Critical kinetics near gelation, J. Phys. A: Math. Gen. **15**, 1951 (1982).
[33] P. G. J. van Dongen and M. H. Ernst, Scaling solutions of Smoluchowski's coagulation equation, J. Stat. Phys. **50**, 295 (1988).
[34] G. Breschi and M. A. Fontelos, On global in time self-similar solutions of Smoluchowski equation with multiplicative kernel, IMA J. Appl. Math. **88**, 405 (2023).
[35] K. Hasselmann, On the non-linear energy transfer in a gravity-wave spectrum part 1. General theory, J. Fluid Mech. **12**, 481 (1962).
[36] V. E. Zakharov and N. N. Filonenko, The energy spectrum for stochastic oscillation of a fluid's surface, Dokl. Akad. Nauk. **170**, 1992 (1966).
[37] A. C. Newell and B. Rumpf, Wave turbulence, Annu. Rev. Fluid Mech. **43**, 59 (2011).
[38] S. Nazarenko, *Wave Turbulence* (Springer, Heidelberg, 2011).
[39] D. V. Semikoz and I. I. Tkachev, Kinetics of Bose condensation, Phys. Rev. Lett. **74**, 3093 (1995).
[40] R. Lacaze, P. Lallemand, Y. Pomeau, and S. Rica, Dynamical formation of a Bose–Einstein condensate, Physica D **152–153**, 779 (2001).
[41] B. V. Semisalova, V. N. Grebenevb, S. B. Medvedev, and S. V. Nazarenko, Numerical analysis of a self-similar turbulent flow in Bose-Einstein condensates, Commun. Nonlinear Sci. Numer. Simulat. **102**, 105903 (2021).